J Mater Sci (2016) 51:6876–6885

Fabrication, analysis and characterization of $Cu_2Zn_{1-x}Cd_xSnS_4$ quinternary alloy nanostructures deposited on GaN

A. S. Ibraheam[1], Y. Al-Douri[1,2,*], U. Hashim[1], Deo Prakash[3], K. D. Verma[4], and M. Ameri[5]

[1] Institute of Nano Electronic Engineering, University Malaysia Perlis, 01000 Kangar, Perlis, Malaysia
[2] Physics Department, Faculty of Science, University of Sidi Bel-Abbès, 22000 Sidi Bel Abbès, Algeria
[3] School of Computer Science & Engineering, Faculty of Engineering, SMVD University, Kakryal, Katra, Jammu and Kashmir 182320, India
[4] Material Science Research Laboratory, Department of Physics, S. V. College, Aligarh, Uttar Pradesh 202001, India
[5] Laboratoire Physico-Chimie des Matériaux Avancés (LPCMA), Université Djilali Liabès de Sidi Bel-Abbès, 22000 Sidi Bel Abbès, Algeria

Received: 14 February 2016
Accepted: 11 April 2016
Published online: 19 April 2016

© Springer Science+Business Media New York 2016

ABSTRACT

The $Cu_2Zn_{1-x}Cd_xSnS_4$ quinternary alloy nanostructures with different Cd concentrations were prepared using spin coating technique on GaN substrate. The structural properties of $Cu_2Zn_{1-x}Cd_xSnS_4$/GaN were investigated by X-ray diffraction (XRD) and field emission-scanning electron microscope. XRD studies indicated that kesterite phase of Cu_2ZnSnS_4 and stannite phase of Cu_2CdSnS_4 were formed. The optical properties were studied through photoluminescence technique, and indicated that the band gap shifted as Cd concentration increases from 1.75 eV in Cu_2ZnSnS_4 to 1.65 eV in Cu_2CdSnS_4. The electrical characterization of the Ag/n-GaN/$Cu_2Zn_{1-x}Cd_xSnS_4$/Ag diode through current to voltage (*I–V*) characterization showed the highest photoresponse of (value if any) at $Cu_2Zn_{0.4}Cd_{0.6}SnS_4$ composition.

Introduction

Stoichiometric Cu_2–II–IV–VI_4 (II = Zn, Cd, Hg; IV = Si, Ge, Sn; VI = S, Se, Te) chalcogenide semiconductors have drawn the increasing interest during the past few decades due to their potential applications in photovoltaic [1–4] and thermoelectric [5, 6] devices. Especially, ongoing efforts have been devoted to the Cu_2ZnSnS_4 (CZTS) solar cells in view of their power conversion efficiencies, even as high as 12.0 % [3]. The fabrication techniques for CZTS thin films become flourishing correspondingly, e.g. sputtering [7], thermal evaporation [8, 9], chemical vapour deposition [10], atomic layer deposition [11], electrodeposition [4], spray coating [2] and spray pyrolysis [12, 13].

Theoretical calculations indicated that the best fit with solar spectrum and the optimal band gap for

Address correspondence to E-mail: yaldouri@yahoo.com

DOI 10.1007/s10853-016-9975-7

absorber materials is around 1.4 eV. To reach the ideal band gap for CZTSSe-based single-junction solar cells, the ratio of S/Se is modified in several studies [14–16]. The synthesis of $Cu_2Cd_xZn_{1-x}SnS_4$ $(0 \le x \le 1)$ (CZCTS) alloy by sol–gel method has been accomplished [17] to achieve the goal of bandgap engineering in Cu_2ZnSnS_4-based solar cells. Ibraheam et al. [17] have reported that the optical band gap of CZCTS alloy can be also modified continuously from 1.55 to 1.09 eV as Cd varies from 0 to 1.

The low-cost Cu_2CdSnS_4 nanocrytal thin film with a stannite structure has been successfully fabricated by Zhao et al. [18]. The selenized $Cu_2CdSn(S,Se)_4$ thin film shows large densely packed grains and has a suitable bandgap value of 1.01 eV. The $Cu_2CdSn(S,Se)_4$ thin-film solar cell with a proof-of-concept power conversion efficiency of 3.1 % was fabricated. Recently, Guo et al. [19] have fabricated Cu_2ZnSnS_4 (CZTS) thin films by sulphurization of direct current and pulse reverse co-electrodeposited CZTS precursors on Mo-coated glass substrates. The CZTS thin film synthesized using pulse reverse co-electrodeposition exhibits homogeneous and large grains, Cu-poor and Zn-rich compositions and free of Cu_2S secondary phase compared with that obtained from direct current co-electrodeposition. By using pulse reverse co-electrodeposition, the performance of pen junction is improved with low diode quality factor (A) and reverse saturation current density (J_0), and the CZTS device first reaches an efficiency of 6.28 % (V_{oc} = 609 mV, J_{sc} = 18.4 mA/cm^2, FF = 56.1 %) threshold, which is higher than that of 4.69 % (V_{oc} = 561 mV, J_{sc} = 16.4 mA/cm^2, FF = 50.9 %) using direct current

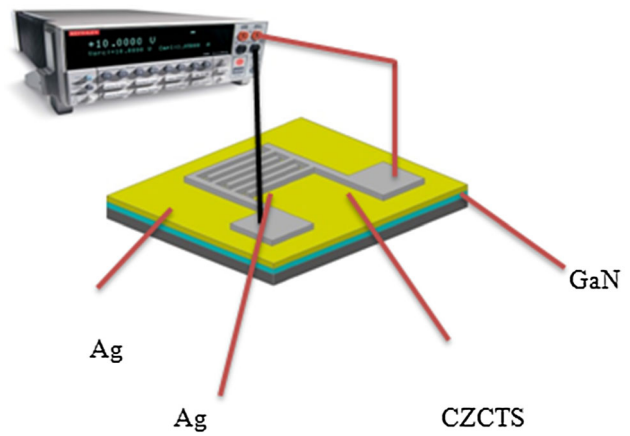

Figure 1 p–n injection.

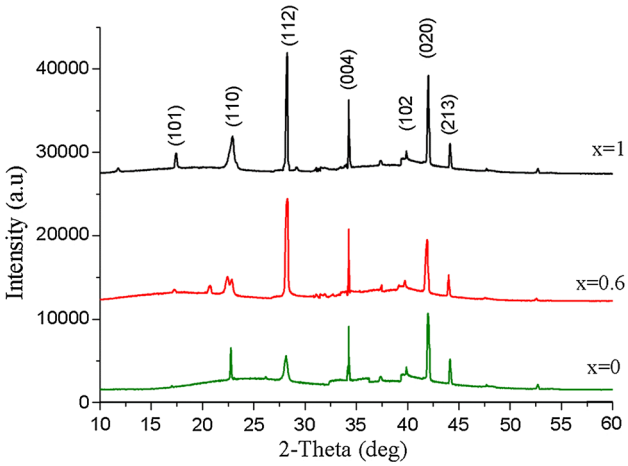

Figure 2 XRD patterns of $Cu_2Zn_{1-x}Cd_xSnS_4$ quinternary alloy nanostructures with different Cd concentrations (x = 0, 0.6, 1).

co-electrodeposition. This result offers a novel research direction for preparing high-efficiency CZTS thin-film solar cells.

Till now, there are no reports on the optical and morphological properties of $Cu_2Zn_{1-x}Cd_xSnS_4$ quinternary alloy nanostructures deposited on n-type GaN substrates; therefore, in this study, high-quality $Cu_2Zn_{1-x}Cd_xSnS_4$ quinternary alloy nanostructures were deposited on GaN substrates by spin coating technique to study the structural properties given by X-ray diffraction (XRD) and field emission-scanning electron microscope (FE-SEM), and optical properties of $Cu_2Zn_{1-x}d_xSnS_4$ quinternary alloy nanostructures by photoluminescence (PL), in addition to investigating the electrical properties of Ag/n-GaN/$Cu_2Zn_{1-x}Cd_xSnS_4$/Ag diode at x = 0, 0.6, 1 for photodetector applications through (I–V) characterization.

Experimental process

Spin coating technique is used to deposit the $Cu_2Zn_{1-x}Cd_xSnS_4$ quinternary alloy nanostructures onto GaN (0001) substrate. First, a solution of $Cu_2Zn_{1-x}Cd_xSnS_4$ precursors was prepared from copper(II) chloride dihydrate, zinc(II) chloride dihydrate, tin (II) chloride dihydrate thiourea, 2-methoxyethanol (2-metho) and monoethanolamine (MEA). The 2-metho and MEA were used as solvent and stabilizer, respectively. The molar ratio of MEA to solution of $Cu_2Zn_{1-x}Cd_xSnS_4$ was at 0.5. The precursor

Table 1 The structural properties of $Cu_2Zn_{1-x}Cd_xSnS_4$ quinternary alloy nanostructures using XRD for different values of x

x	Peak (θ)	Crystallite size (nm)	d_{hkl} (112) (Å)	Lattice constants (Å)	Energy gap (eV)
0	28.19	44.69	3.356	$a = 5.329$ $a = 5.427$* $c = 10.656$ $c = 10.848$*	1.75
0.6	28.15	49.32	3.467	$a = 5.465$ $c = 10.734$	1.68
1	28.07	58.22	3.558	$a = 5.553$ $c = 5.487^{\#}$ $c = 11.956$ $c = 10.845^{\#}$	1.65

* Ref. [21] exp.; # Ref. [22] exp

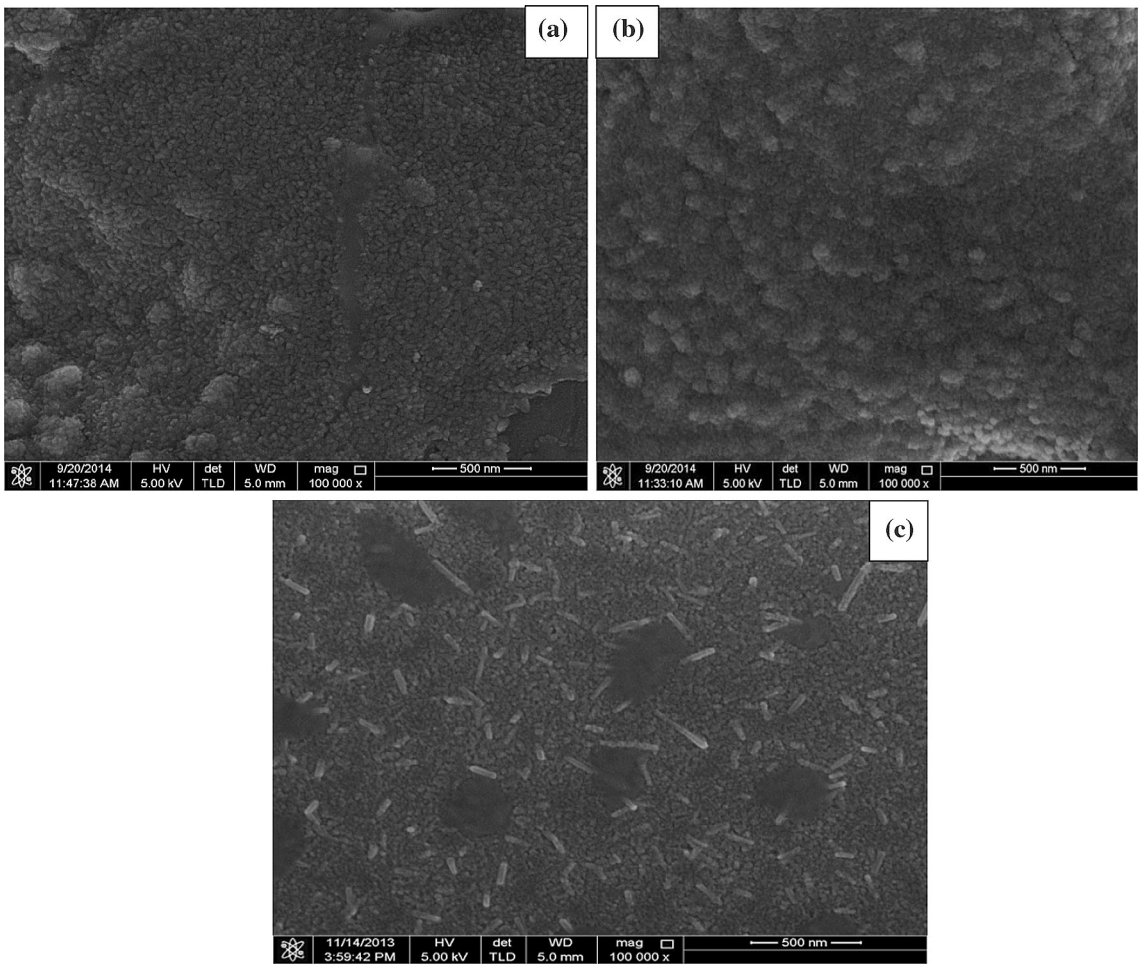

Figure 3 FE-SEM images of $Cu_2Zn_{1-x}Cd_xSnS_4$ quinternary alloy nanostructures for different Cd concentrations **a** 0, **b** 0.6, **c** 1.

solution (0.3 M) was stirred at 50 °C for 3 h to completely dissolve the metals during stirring, and after adding thiourea, the milk solution became yellow and transparent. The molar ratio of Cu, (Zn + Cd), Sn and S in the solution was 2:1:1:4. To obtain solutions with different Cd concentrations (x), the molar ratio of Cd to (Zn + Cd) in the solution varied to give x values of 0, 0.6, 0.8 and 1. The precursor solutions were mixed based on the required ratio of the following formula $Cu_2^{2+}(Zn_{1-x}Cd_x)^{2+}$

Sn^{4+} S_4^{8-}. This means that the solution consisted of two parts of Cu and one part of (Zn,Cd) depending on the value of x, one part Sn and four parts S. The solution was then dropped onto a GaN (0001) substrate (20 mm × 20 mm × 1 mm) rotating at 2500 rpm for 30 s. After deposition by the spin coating, the nanostructures were dried at 250 °C for 80 min on a hot plate. The coating and drying processes were repeated seven times to obtain a film of 1 μm thickness.

The crystal structure of the $Cu_2Zn_{1-x}Cd_xSnS_4$ quinternary alloy nanostructures was examined by X-ray diffraction (XRD; PW 1710 X-ray diffractometer, Phillips, USA) with Cu Kα radiation ($\lambda = 1.54$ Å). The optical properties were measured at room temperature using UV–Visible spectrophotometry (Lambda 950, Perkin Elmer, USA) and photoluminescence spectroscopy (Jobin Yvon model HR 800 UV system, Jobin Yvon, USA) at room temperature using a He–Cd laser ($\lambda = 325$ nm). Surface morphology and grain size were investigated by field emission-scanning electron microscopy (FE-SEM) (NOVA NANO SEM 450, USA). The topography of the films was characterized by atomic force microscopy (AFM) (SII SPI 3800N Probe, Seiko Instruments Inc., USA). Thickness measurement was carried out using the weight method given by

$$t = \frac{\Delta m}{A \times \rho}, \tag{1}$$

where t is thickness, Δm is a difference of substrate weight (substrate after deposition—substrate before deposition), A is area of sample and ρ is the density of deposited material. Finally, heat treatment was conducted in an elevator furnace under N_2 gas flow (5 % gas atmosphere) for 1 h at 300 °C, and after annealing, the samples were cooled to below 40 °C in the chamber. After that, Ag metal contacts were formed on $Cu_2Zn_{1-x}Cd_xSnS_4$ quinternary alloy nanostructures with Cd concentration equals 0, 0.6, 1. PVD-HANDY/2STE (Vaksis Company, USA) vacuum thermal evaporation in the pressure of 4.5×10^5 Torr was used for deposition on GaN, and the contacts were formed in the form of zig-zag with

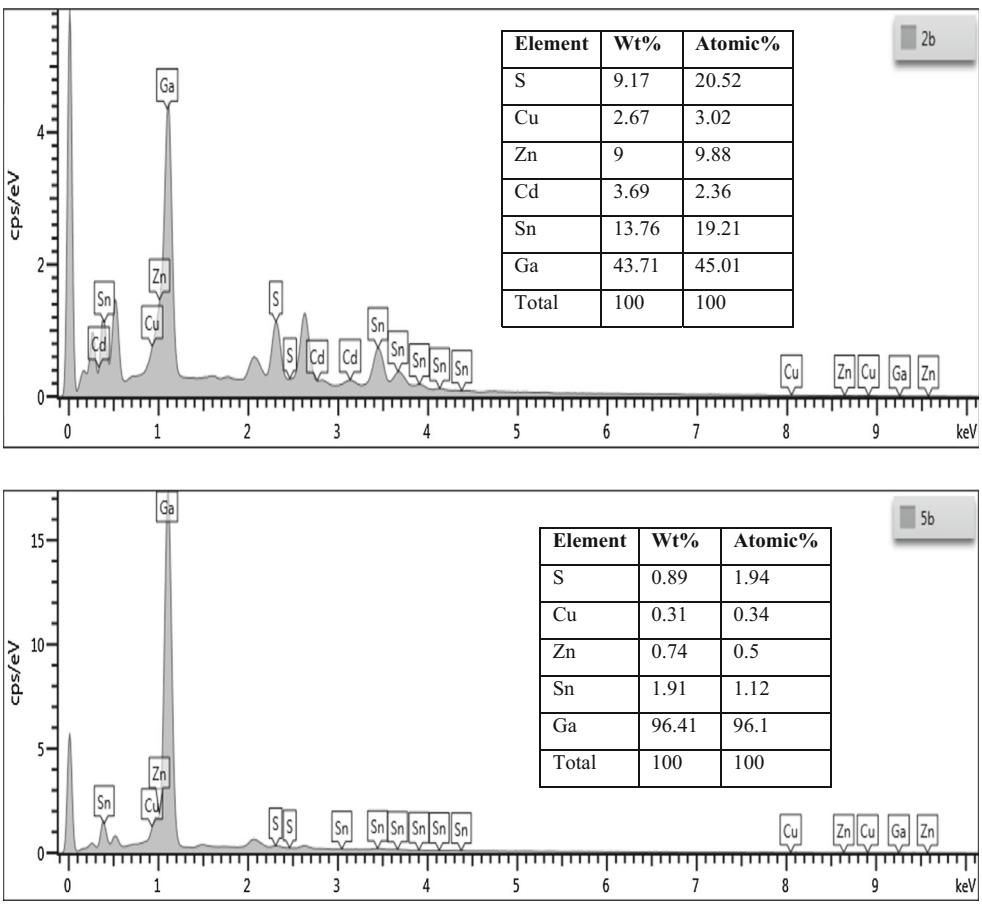

Figure 4 EDX of $Cu_2Zn_{1-x}Cd_xSnS_4$ quinternary alloy nanostructures at different Cd concentrations $x = 0, 0.6, 1$.

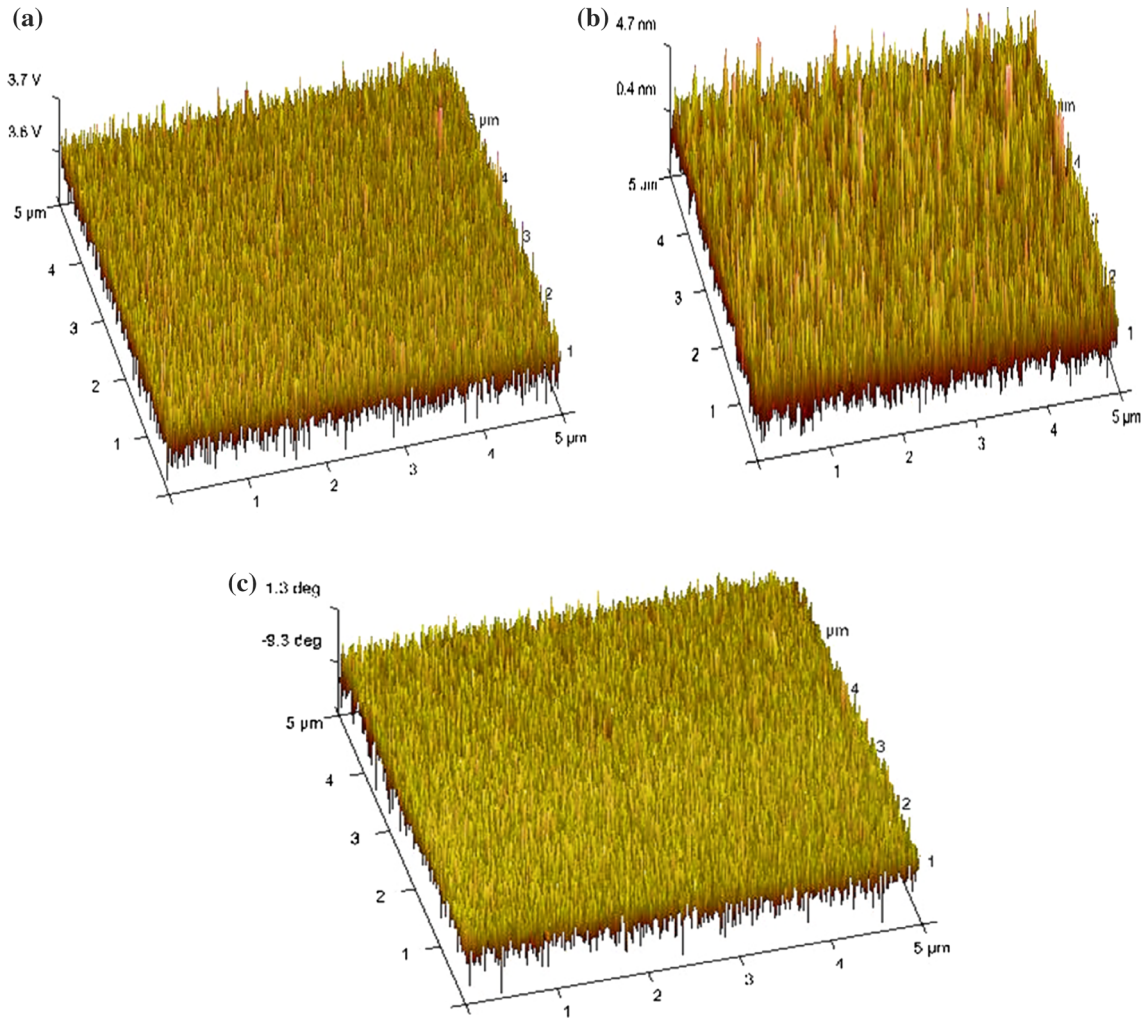

Figure 5 3D AFM images of $Cu_2Zn_{1-x}Cd_xSnS_4$ quinternary alloy nanostructures with different Cd contents **a** 0, **b** 0.6, **c** 1.

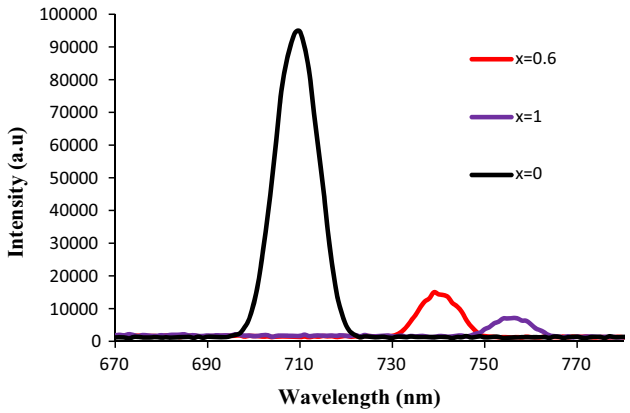

Figure 6 The photoluminescence (PL) of $Cu_2Zn_{1-x}Cd_xSnS_4$ quinternary alloy nanostructures with different Cd concentrations.

5 mm length and 100 nm thickness as shown in Fig. 1. The contact area of the diode was found to be 3.14×10^2 cm^2. For the current to voltage (I–V) characterization, the fabricated device was connected in parallel with the Kiethly (2400 source meter, USA). The reading was recorded from −6 to 6 V. For current to time (I–t) analysis, the device was connected in series with the multimeter and the value was recorded by switching the LED on and off. The wavelength and power of the LED used for conducting the experiment were 490 nm wavelength and 3 mW power, respectively.

Results and discussion

The typical XRD pattern of the $Cu_2Zn_{1-x}Cd_xSnS_4$ quinternary alloy nanostructures is shown in Fig. 2. It can be seen that the major diffraction peaks at

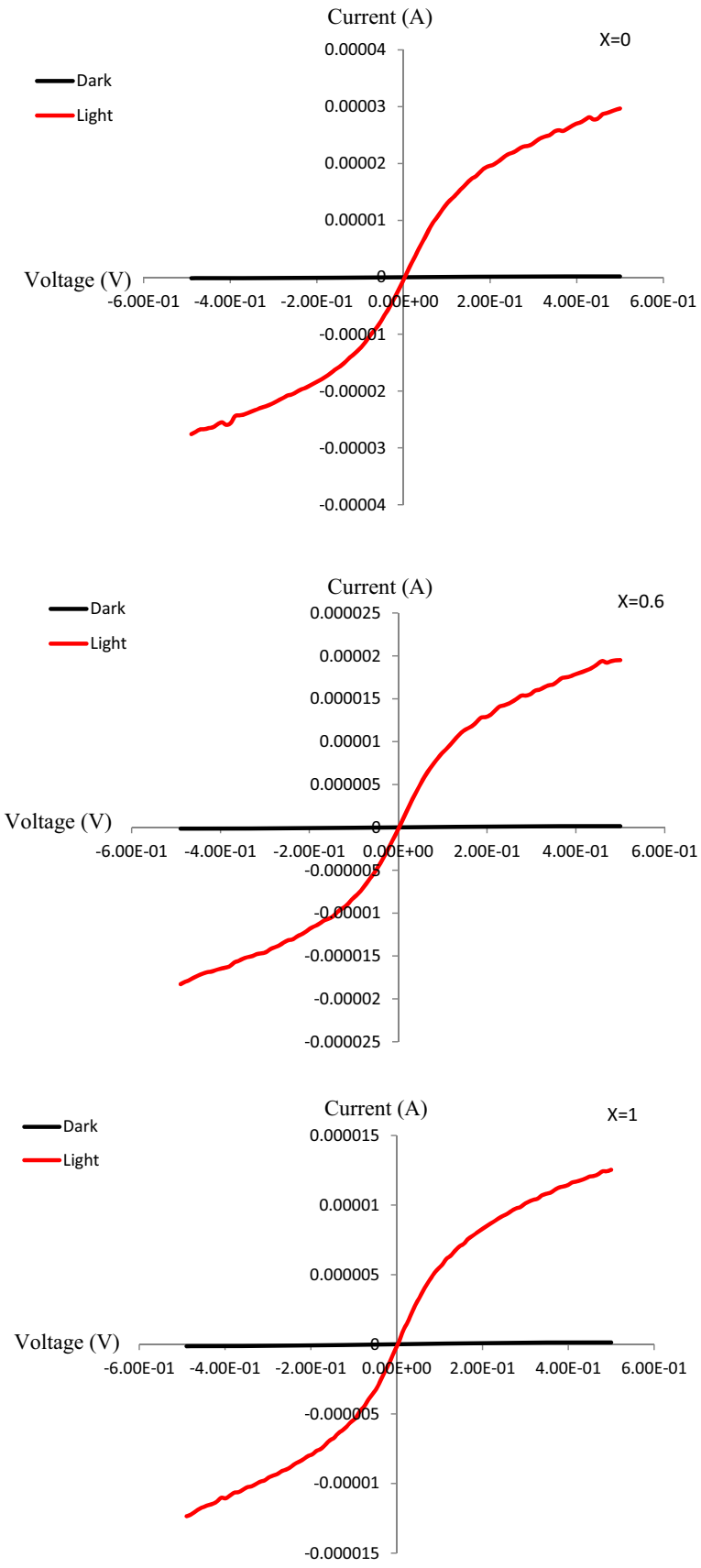

Figure 7 *I–V* characteristics in dark and under illuminating were 490 nm and 3 mW for $Cu_2Zn_{1-x}Cd_xSnS_4$ quinternary alloy nanostructures with Cd concentration values $x = 0$, 0.6, 1.

Table 2 Photoresponse properties of the Ag/GaN/$Cu_2Zn_{1-x}Cd_xSnS_4$/Ag heterojunction at wavelength 490 nm

X	I_{dark} (A) ($\times 10^{-7}$)	I_{ph} (A)	I_{ph}/I_{dark}	S_{ph} (%)
0	1.28753	1.24233×10^{-5}	3.82	98.9636
0.6	1.36638	1.92087×10^{-3}	34.01	99.9982
1	1.49471	2.88917×10^{-5}	6.67	99.4826

$2\theta = 17.46°$, 22.93°, 28.26°, 34.39°, 39.85° and 44.13° can be attributed to the (101), (110), (112), (004), (102) and (213) plans of kesterite phase of Cu_2ZnSnS_4 and stannite phase of Cu_2CdSnS_4. Owing to the presence of four or five elements in the materials, there was a possibility for the secondary phases like SnS, attributed to the (110) was observed at $2\theta = 41.99°$ corresponding to JSPDS cards (00-001-1244). According to the Debye–Scherrer formula, (112) peak was calculated to increase the accuracy, and the average crystallite size of the CZCTS nanostructures can be presented in Table 1. The relatively intense and sharper (112) and (200) diffraction peaks were observed for nanostructures deposited at $x = 0.6$ and 1. However, when the concentration of Cd was further increased to 0.6 and 1, the intensity of diffraction peaks increases, which indicates that the crystallinity increase with increasing in concentration of Cd. The peak (112) was shifted to the lower angle side with increasing Cd concentration in the CZCTS solid solutions, which was attributed to the increasing lattice constant. This was due to the radius of Cd ion (1.53 Å) which is larger than that of Zn (1.33 Å) as supported by previous work [17]. The simplest possibility is that Cd substitutes other metals at their sites in crystal lattice of $Cu_2Cd_xZn_{1-x}SnS_4$ quinternary alloy nanostructures. As the theoretical calculated substitution energies of Cd atoms at Cu, Sn and Zn atom sites in CZCTS lattice are E_{sub} (Cd_{Cu}) = 0.69 eV, E_{sub} (Cd_{Sn}) = 1.07 eV and E_{sub} (Cd_{Zn}) = 0.53 eV [20], the most likely is the isoelectronic substitution of Cd at the Zn site. Lattice constants a and c were calculated from XRD data for the (112) plane, which are given in Table 1.

Figure 3 shows FE-SEM micrographs of $Cu_2Zn_{1-x}Cd_xSnS_4$ quinternary alloy nanostructures with Cd concentration equals (a) 0, (b) 0.6 and (c) 1. From FE-SEM images, the obtained $Cu_2Zn_{1-x}Cd_xSnS_4$ layer on GaN substrate was found to be homogeneous with good adherence to the substrate. $Cu_2Zn_{1-x}Cd_xSnS_4$ quinternary alloy nanostructures are clearly discernible, indicating an isolated grain growth at the surface. With the addition of Cd, the shape of the grains changed significantly (Fig. 3). The grain shape becomes rounder as well as bigger for 0.6. The presence of nanowire rod shaped when $x = 1$ might lead to the formation of more densely packed nanostructures with less porosity.

The elemental analysis of $Cu_2Zn_{1-x}Cd_xSnS_4$ quinternary alloy nanostructures with different Cd concentrations was investigated using EDAX and their compositions are illustrated in Fig. 4. The presence of Cu, Zn, Cd, Sn and S elements is confirmed by EDAX analysis. Furthermore, it is also interesting to note that the composition of Zn in $Cu_2Zn_{1-x}Cd_xSnS_4$ varies upon increasing the Cd concentration. The nanostructures were copper poor and zinc rich at x (0, 0.6) concentrations [23, 24].

Figure 5 represents the three-dimensional topographic AFM images $Cu_2Zn_{1-x}Cd_xSnS_4$ quinternary alloy nanostructures with Cd concentration equals 0, 0.6 and 1. For a detailed study on average roughness properties of $Cu_2Zn_{1-x}Cd_xSnS_4$ with Cd concentration, line profiles were recorded. From the line profile analysis, the calculated average roughness values are 3.56, 4.356 and 5.167 nm for $x = 0$, 0.6, 1, respectively. Minimum average surface roughness value is 3.56 nm. It was found that the incorporation of Cd results in the increasing of surface roughness.

PL spectra of CZCTS quinternary alloy nanostructures with different Cd concentrations measured at room temperature are shown in Fig. 6. PL spectra consist of one broad asymmetric PL band at 1.75 eV in Cu_2ZnSnS_4 and at 1.65 eV in Cu_2CdSnS_4 as given in Table 1. A shift of PL band of $Cu_2Zn_{1-x}Cd_xSnS_4$ quinternary alloy nanostructures towards highest wavelengths with increasing Cd concentration is observed in the region $0 \leq x \leq 1$. This shifting is due to the substitution of Zn atoms with Cd atoms to produce a lower energy gap [25, 26].

Figure 7 shows that the I–V characteristics from −6 to 6 V of $Cu_2Zn_{1-x}Cd_xSnS_4$ quinternary alloy nanostructures with Cd concentration values $x = 0$, 0.6, 1 measured in the dark and under illuminating were 490 nm and 3 mW. The difference between I_{dark} and I_{ph} is increased in $Cu_2Zn_{0.4}Cd_{0.6}SnS_4$ heterojunction compared with Cu_2ZnSnS_4 ($x = 0$) heterojunction. The photosensitivities of the heterojunction were calculated by

$$S = \frac{I_{ph} - I_{dark}}{I_{dark}} \times 100\ \%. \quad (2)$$

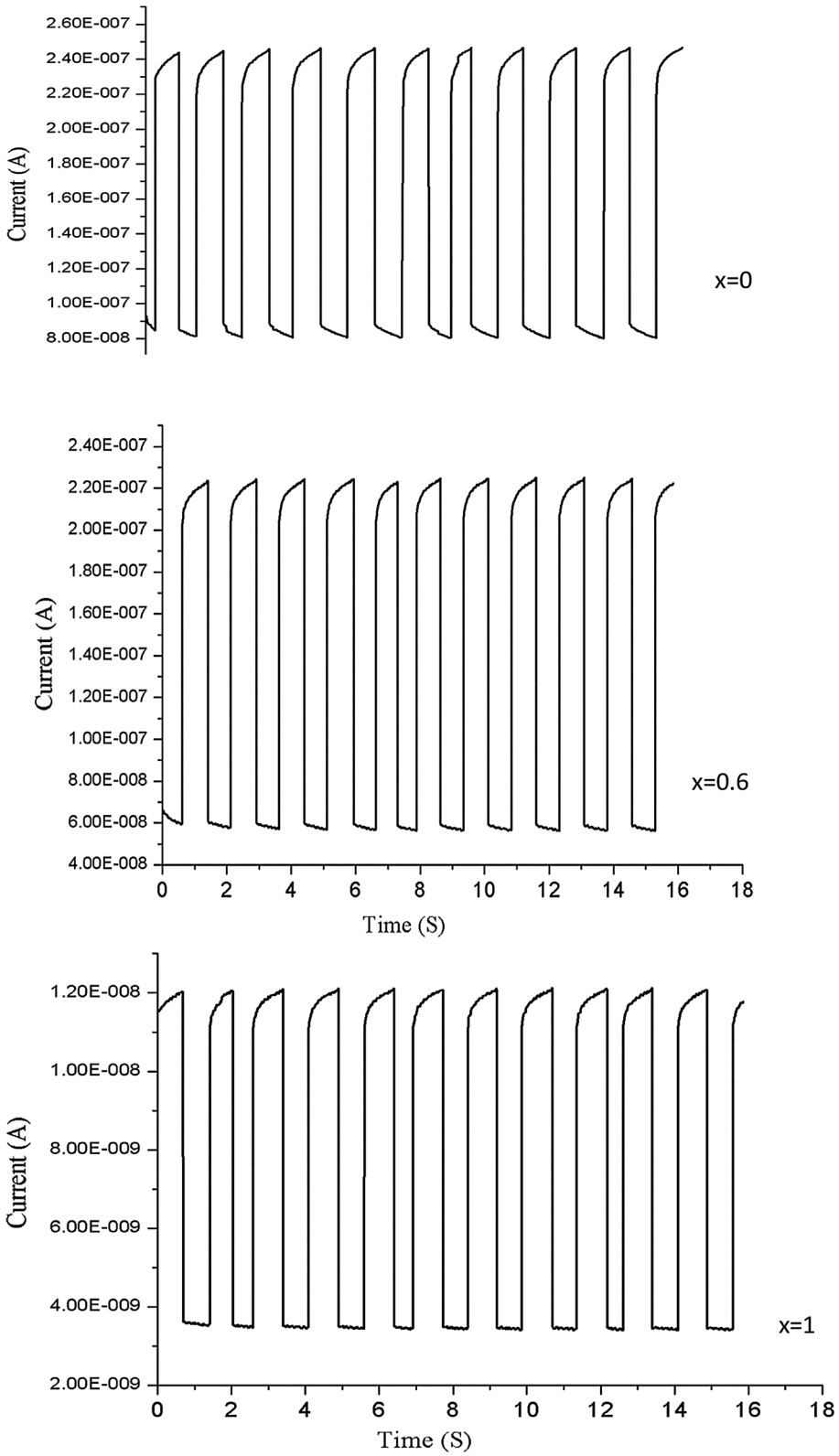

Figure 8 Photocurrent response spectra of Ag/GaN/$Cu_2Zn_{1-x}Cd_xSnS_4$/Ag heterojunction at different Cd concentrations, $x = 0$, 0.6, 1, under illuminating light were 490 nm and 3 mW turned on and off repeatedly.

Table 3 Response and decay time corresponding to I_{ph}/I_{dark} ratio of Ag/GaN/$Cu_2Zn_{1-x}Cd_xSnS_4$/Ag diode

x	Response time (t_{Res}) (s)	Decay time (t_{Rec}) (s)	I_{ph}/I_{dark}
0	0.01274	0.01083	2.6
0.6	0.02654	0.01064	3.6
1	0.01331	0.0106	3

Based on the *I–V* curve (Fig. 7) and Eq. (2), the I_{dark} and I_{ph} and S_{ph} are listed in Table 2. Figure 7 shows that the photosensitivity increases with increasing Cd concentration to 99.9982 for $x = 0.6$ and decreased to 99.4826 for $x = 1$. There is no significant difference in photosensitivity when the concentration of Cd increases.

To confirm the better performance of the heterojunction and reproducibility of Ag/GaN/$Cu_2Zn_{1-x}Cd_xSnS_4$/Ag device, it was examined by cyclically switching the white light on and off. Figure 7 shows the I_{ph} as a function of time intervals (*I–t*) of $Cu_2Zn_{1-x}Cd_xSnS_4$ quinternary alloy nanostructures at $x = 0$, 0.6, 1. I_{ph} sharply increases/decreases to reach the maximum/minimum under 490 nm light on/off. The $Cu_2Zn_{1-x}Cd_xSnS_4$ quinternary alloy nanostructures at $x = 0.6$ (Fig. 7b) show better performance than at $x = 0$, 1 (Fig. 8). The result indicated an improvement with increasing Cd concentration, $x = 0.6$. The I_{ph}/I_{dark} ratio was 2.6, 3.6 and 3 for $x = 0$, 0.6 and 1, respectively, as given in Table 3. The calculated response time (t_{Res}) and decay time (t_{Rec}) using 490 nm and 3 V show that all values decreased with increasing of Cd concentration indicating an improved photoresponse. The performance of $Cu_2Zn_{1-x}Cd_xSnS_4$ quinternary alloy nanostructures shows t_{Res} (0.02654) and t_{Rec} (0.01064) for $x = 0.6$ (Table 3).

Conclusion

The $Cu_2Zn_{1-x}Cd_xSnS_4$ quinternary alloy nanostructures were prepared on *n*-GaN substrate using spin coating technique. XRD results revealed that the as-prepared CZCTS exhibits impurity-free kesterite phase of Cu_2ZnSnS_4 and stannite phase of Cu_2CdSnS_4 in polycrystalline nature with the crystallite sizes between 44.69 and 58.22 nm. The band gap was found to decrease with increasing Cd concentrations. It was found that the incorporation of Cd results in an increasing of surface roughness of $Cu_2Zn_{1-x}Cd_xSnS_4$ nanostructures from 3.56 to 4.356 nm. Under illumination densities, the *n*-GaN/CZCTS junction exhibited good photoconductivity. The I_{on}/I_{off} ratios confirmed the photosensitivity of the produced structure. Photocurrent measurements showed the highest photoresponse for $Cu_2Zn_{0.4}Cd_{0.6}SnS_4$ quinternary alloy nanostructures.

Acknowledgements

Y.A. would like to thank University Malaysia Perlis for grant No. 9007-00185. K.D.V. would like to acknowledge U.G.C., New Delhi, India for providing financial assistance in the form of Major Research Project [Code: 42-856/2013(SR)].

References

[1] Cao YY, Denny MS, Caspar JV, Farneth WE, Guo QJ, Ionkin AS, Johnson LK, Lu MJ, Malajovich I, Radu D, Rosenfeld HD, Choudhury KR, Wu W (2012) High-efficiency solution-processed $Cu_2ZnSn(S, Se)_4$ thin-film solar cells prepared from binary and ternary nanoparticles. J Am Chem Soc 134:15644–15647

[2] Carrete A, Shavel A, Fontane X, Montserrat J, Fan JD, Ibanez M, Saucedo E, Perez-Rodriguez A, Cabot A (2013) Antimony-based ligand exchange to promote crystallization in spray-deposited $Cu_2ZnSnSe_4$ solar cells. J Am Chem Soc 135:15982–15985

[3] Winkler MT, Wang W, Gunawan O, Hovel HJ, Todorov TK, Mitzi DB (2014) Optical designs that improve the efficiency of $Cu_2ZnSn(S, Se)_4$ solar cells. Energy Environ Sci 7:1029–1036

[4] Ahmed S, Reuter KB, Gunawan O, Guo L, Romankiw LT, Deligianni H (2012) A high efficiency electrodeposited Cu_2ZnSnS_4 solar cell. Adv Energy Mater 2:253–259

[5] Fan FJ, Yu B, Wang YX, Zhu YL, Liu XJ, Yu SH, Ren ZF (2011) Colloidal synthesis of $Cu_2CdSnSe_4$ nanocrystals and hot-pressing to enhance the thermoelectric figure-of-merit. J Am Chem Soc 133:15910–15913

[6] Ibanez M, Zamani R, LaLonde A, Cadavid D, Li WH, Shavel A, Arbiol J, Morante JR, Gorsse S, Snyder GJ, Cabot A (2012) $Cu_2ZnGeSe_4$ nanocrystals: synthesis and thermoelectric properties. J Am Chem Soc 134:4060–4063

[7] Scragg JJ, Ericson T, Fontane X, Izquierdo-Roca V, Perez-Rodriguez A, Kubart T, Edoff M, Platzer-Bjorkman C (2014) Rapid annealing of reactively sputtered precursors for Cu_2ZnSnS_4 solar cells. Prog Photovolt 22:10–17

[8] Schubert BA, Marsen B, Cinque S, Unold T, Klenk R, Schorr S, Schock HW (2011) Cu_2ZnSnS_4 thin film solar cells by fast coevaporation. Prog Photovolt 19:93–96

[9] Shin B, Gunawan O, Zhu Y, Bojarczuk NA, Chey SJ, Guha S (2013) Thin film solar cell with 8.4% power conversion efficiency using an earth-abundant Cu_2ZnSnS_4 absorber. Prog Photovolt 21:72–76

[10] Ramasamy K, Malik MA, O'Brien P (2011) The chemical vapor deposition of Cu_2ZnSnS_4 thin films. Chem Sci 2:1170–1172

[11] Thimsen E, Riha SC, Baryshev SV, Martinson ABF, Elam JW, Pellin MJ (2012) Atomic layer deposition of the quaternary chalcogenide Cu_2ZnSnS_4. Chem Mater 24: 3188–3196

[12] Nie L, Liu S, Chai Y, Yuanm R (2015) Spray pyrolysis deposition and photoresponse of Cu_2CdSnS_4 thin films. J Anal Appl Pyrol 112:363–368

[13] Daranfed W, Aida MS, Attaf N, Bougdira J, Rinnert H (2012) Cu_2ZnSnS_4 thin films deposition by ultrasonic spray pyrolysis. J Alloys Compd 542:22–27

[14] Timmo K, Altosaar M, Raudoja J, Muska K, Pilvet M, Kauk M, Varema T, Danilson M, Volobujeva O, Mellikov E (2010) Sulfur-containing $Cu_2ZnSnSe_4$ monograin powders for solar cells. Sol Energy Mater Sol Cells 94:1889

[15] Cao Y, Xiao Y, Jung J-Y, Um H-D, Jee S-W, Choi HM, Bang JH, Lee J-H (2013) Highly electrocatalytic $Cu_2ZnSn(S_{1-x}Se_x)_4$ counter electrodes for quantum-dot-sensitized solar cells. Appl Mater Interfaces 5:479

[16] Wang Y-P, Levcenco S, Dumcenco DO, Huang Y-S, Ho C-H, Tiong K-K (2013) Composition dependent band gaps of single crystal $Cu_2ZnSn(S_xSe_{1-x})_4$ solid solutions. Solid State Phenom 194:139–144

[17] Ibraheam AS, Al-Douri Y, Hashim U, Ghezzar MR, Addou A (2015) Waleed K. Ahmed. Cadmium effect on optical properties of $Cu_2Zn_{1-x}Cd_xSnS_4$ quinternary alloys nanostructures. Sol Energy 114:39–50

[18] Zhao W, Wang G, Tian Q, Huang L, Gao S, Pan D (2015) Solution-processed $Cu_2CdSn(S, Se)_4$ thin film solar cells. Sol Energy Mater Sol Cells 133:15–20

[19] Guo Min, Zhu Xiurong, Li Hejun (2016) Comparative study of Cu_2ZnSnS_4 thin film solar cells fabricated by direct current and pulse reverse co-electrodeposition. J Alloy Compd 657:336–340

[20] Maeda T, Nakamura S, Wada T (2012) First-principles study on Cd doping in Cu_2ZnSnS_4 and $Cu_2ZnSnSe_4$. Jpn J Appl Phys 51:10NC11–10NC16

[21] Suehiro S, Horita K, Kumamoto K, Yuasa M, Tanaka T, Fujita K, Shimanoe K, Kida T (2014) Solution-processed Cu_2ZnSnS_4 nanocrystal solar cells: efficient stripping of surface insulating layers using alkylating agents. J Phys Chem C 118:804–810

[22] Nie L, Liu S, Chai Y, Yuan R (2015) Spray pyrolysis deposition and photoresponse of Cu_2CdSnS_4 thin films. J Anal Appl Pyrolysis 112:363–368

[23] Kahraman S, Cetinkaya S, Cetinkara HA, Guder HS (2014) Effects of diethanolamine on sol–gel–processed Cu_2ZnSnS_4 photovoltaic absorber thin films. Mater Res Bull 50:165–171

[24] Fischereder A, Rath T, Haas W, Amenitsch H, Albering J, Meischler D, Larissegger S, Edler M, Saf R, Hofer F, Trimmel G (2010) Investigation of Cu_2ZnSnS_4 formation from metal salts and thioacetamide. Chem Mater 22: 3399–3406

[25] Lee KH, Kim HY, Bang HJ, Jung YH, Lee SG (2003) The change of bead morphology formed on electrospun polystyrene fibers. Polymer 44:4029–4034

[26] Luque PA, Quevedo-Lopez MA, Olivas A (2013) Influence of deposition time on ZnS thin film growth over SiO_2 and glass substrates. Mater Lett 106:49–51